Ab initio study of the spin-orbit coupling between the A1Σ +u and b 3Πu electronic states of Na2

Satchin Soorkia, Frederic Le Quere, Céline Léonard, Detlev Figgen

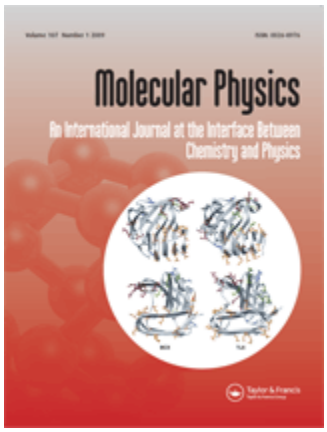

Ab initio study of the spin-orbit coupling between the $A^1\Sigma^+_u$ and $b^3\Pi_u$ electronic states of Na_2

Journal:	*Molecular Physics*
Manuscript ID:	TMPH-2006-0054.R2
Manuscript Type:	Full Paper
Date Submitted by the Author:	28-Nov-2006
Complete List of Authors:	SOORKIA, Satchin; CEA LE QUERE, Frederic; Université de Marne la Vallée, Laboratoire de Chimie Théorique leonard, celine; Universite de Marne la Vallee Figgen, Detlev; Universität Stuttgart, Institut für Theoretische Chemie
Keywords:	spin orbit coupling, Wave packet propagation, Dipole moment

Ab initio study of the spin-orbit coupling between the $A^1\Sigma_u^+$ and $b^3\Pi_u$ electronic states of Na_2

S. Soorkia[a], F. Le Quéré[b], C. Léonard[b] and D. Figgen[c]

[a] Laboratoire Francis PERRIN - Bât 522 CEA/DSM/DRECAM/SPAM - CNRS URA 2453 - 91191 Gif-sur-Yvette CEDEX - France

[b] Université de Marne la Vallée, Laboratoire de Chimie Théorique, EA 2180, 5 bd Descartes, Champs-sur-Marne - 77454 Marne la Vallée Cedex 2 - France

[c] Institut für Theoretische Chemie, Universität Stuttgart, Pfaffenwaldring 55, 70569 Stuttgart, Germany

Abstract

Accurate *ab initio* representation of the ground $X^1\Sigma_g^+$, excited $A^1\Sigma_u^+$ and $b^3\Pi_u$ electronic states of Na_2 are computed along with the transition dipole moment between $X^1\Sigma_g^+$ and $A^1\Sigma_u^+$ and the spin-orbit coupling term between $A^1\Sigma_u^+$ and $b^3\Pi_u$. These data are used to simulate an experiment involving these three states to investigate the effect of spin-orbit coupling on the dynamics of a wave packet oscillating on the $A^1\Sigma_u^+$ state (S. Rutz *et al. Chem. Phys. Lett.*, **257**, 365-373 (1996)).

Corresponding author :
Dr. Frédéric LE QUERE
Université de Marne la Vallée
Laboratoire de Chimie Théorique - Bâtiment Lavoisier
5 boulevard Descartes - Champs sur Marne
77454 MARNE LA VALLEE CEDEX 2
FRANCE
Tel : +33.1.60.95.73.05
Fax : +33.1.60.95.73.20
Email : lequere@univ-mlv.fr

1 Introduction

Electronic structure calculations have reached such a level of precision that a totally *ab initio* treatment can be envisioned to simulate experiments involving several electronic states that may be coupled. The increasing use of laser pulses in chemical physics [1, 2, 3], in our case to induce transition between electronic states, requires a complete wave packet dynamical treatment of the system in order to fully describe the simulated process. The couplings between electronic states, such as spin-orbit interaction, are often very weak but play an important role in a lot of experiments [4]. Extracting informations on these couplings via analysis of experimental data generally requires a huge amount of work [5, 6] while they can be readily obtained from theory.

In this paper, we present such an *ab initio* "theoretical experiment" that will try to reproduce experimental data from Rutz *et al.*[4] involving three electronic states of Na_2. The ground state, $X^1\Sigma_g^+$, is coupled to the $A^1\Sigma_u^+$ state by a laser pulse interacting with the transition dipole moment between these two states, and the $A^1\Sigma_u^+$ state is coupled to the $b^3\Pi_u$ state by spin-orbit interaction. The full description of the experiment requires a precise determination of the electronic states, of the transition dipole moment and of the spin-orbit coupling, computed from electronic structure theory and a time dependent simulation of the evolution of the nuclear wave packet from which the observables of interest will be computed. Na_2 has been the subject of numerous experimental and theoretical studies: the electronic potential energy functions have been derived from *ab initio* studies by several authors [7, 8] and Rydberg-Klein-Rees (RKR) type potentials have been built from experimental data [9, 10, 11]. Transition dipole moments are also available from theoretical [12] and experimental [13] sources. The interaction between the $A^1\Sigma_u^+$ and $b^3\Pi_u$ states due to the spin-orbit coupling has been deeply studied. Stolyarov *et al.* [14] observed this interaction in g factors. Dulieu and Julienne [15] predicted and Effantin *et al.* [5] observed perturbations in the spectra of these coupled states, however we did not find in the literature any coordinate dependent spin-orbit coupling function. All these references give accurate information concerning our "theoretical experiment" but we chose to compute all the needed electronic structure data in order to ensure the global coherence of our calculations and to determine the complete spin-orbit coupling function. However, we compared our results to all available previous calculation.

For the nuclear motion study, the time dependent wave packet is obtained from the Schrödinger equation

$$\hat{H}\psi(t) = i\hbar\frac{\partial\psi(t)}{\partial t}$$

Where the time dependent hamiltonian, $\hat{H}$ is the sum

$$\hat{H} = \hat{H}_e + \hat{H}_{SO} + \hat{T} - \hat{\vec{\mu}}.\vec{E}(t)$$

In the second section of this article, we will describe the electronic structure calculation and derive representations for the scalar-relativistic electronic hamiltonian, $\hat{H}_e$, the spin-orbit interaction term $\hat{H}_{SO}$ and the transition dipole moment operator $\hat{\vec{\mu}}$. In the third section we will compute bound vibrational states of these electronic states. They will be used in the last section where the full time dependent Schrödinger equation will be solved to simulate the experiment.

2 Electronic structure

The electronic energies were computed using the MOLPRO package[16] for internuclear distances in the range of $3 < r < 20$ bohr. The 10 core electrons of each Na atom are replaced by the effective core potential (ECP) developed by Fuentealba *et al.* [17]. The valence electron is represented by 8 s, 6 p and 1 d even tempered basis functions optimized with the ECP. The core-valence correlation is added by the corresponding core polarisation potential (CPP). The energy of each electronic state ($X^1\Sigma_g^+$, $A^1\Sigma_u^+$, $b^3\Pi_u$) and the transition dipole moment for the transition $X^1\Sigma_g^+$ - $A^1\Sigma_u^+$ are determined using the internally contracted MRCI [18, 19] where the reference comes from a MCSCF [20, 21] calculation with a molecular active space formed by all the valence plus the $4s$ and $4p$ orbitals of the two Na atoms. In this MCSCF step, the two electronic components of $b^3\Pi_u$ were averaged together, as well as the $X^1\Sigma_g^+$ and $A^1\Sigma_u^+$ electronic states.

The spin-orbit coupling terms are the matrix elements of the spin-orbit part of the pseudopotentials, $\hat{H}^{SO}$, evaluated in the basis set formed by the MRCI electronic wavefunctions of $A^1\Sigma_u^+$ and $b^3\Pi_u$. As references, the MRCI calculations used the MCSCF wavefunctions determined with an active space built with the valence orbitals. For these calculations, the same ECP as above is used without the CPP part but with inclusion of an accompanying spin-orbit potential that was adjusted.

Since the one-component ECP of Fuentealba *et al.* was adjusted to experimental energy data, the terms of the spin-orbit ECP were also adjusted to experimental spin-orbit splittings. We used the spin-orbit splittings of the $3p$ and $3d$ configuration [22] as reference data for the adjustment of the p- and d-term, respectively; both adjustments were done seperately. The spin-orbit terms were adjusted in two-component valence average-level calculations with a formally non-relativistic Hamiltonian (including the ECP) for these configurations; this was done in numerical calculations

using the GRASP code [23]. By this method we generate two-component pseudopotentials $V_{l,l+1/2}$ and $V_{l,l-1/2}$ from which the spin-orbit potential $\hat{V}^{SO}$ can easily be obtained:

$$\hat{V}^{SO} = \sum_{l=1}^{2} \frac{l}{2l+1}(V_{l,l+1/2} - V_{l,l-1/2})\mathcal{P}_l \hat{\mathbf{l}} \cdot \hat{\mathbf{s}} \mathcal{P}_l$$

$\mathcal{P}_l$ is the projetion operator on the Hilbert subspace of angular symmetry l:

$$\mathcal{P}_l = \sum_{m_l=-l}^{l} |lm_l\rangle \langle lm_l|$$

In accordance with the one-component ECP that consists of simple Gaussians, the terms of the spin-orbit potentials $\Delta V_l = V_{l,l+1/2} - V_{l,l-1/2}$ were also chosen to be simple Gaussians; moreover, we fixed the exponents of the spin-orbit terms to the exponents of the respective one-component term and solely optimized the coefficients of the Gaussian functions. Table 1 shows the exponents, B and coefficients, β of both the one-component and the spin-orbit potential.

==========

Table 1 near here

==========

We consider the following spin-orbit matrix elements

$$LS_x = \langle {}^1\Sigma_u^+, M_S = 0 | \hat{H}_{SO} | {}^3\Pi_{uy}, M_S = 1 \rangle$$
$$LS_y = \langle {}^1\Sigma_u^+, M_S = 0 | \hat{H}_{SO} | {}^3\Pi_{ux}, M_S = 1 \rangle$$
$$LS_z = \langle {}^3\Pi_{ux}, M_S = 1 | \hat{H}_{SO} | {}^3\Pi_{uy}, M_S = 1 \rangle$$

with $\hat{H}_{SO} = \sum_{\lambda=1}^{2} \hat{V}_\lambda^{SO}$ where λ denotes one of the two Na atoms. LS_x and LS_z are pure imaginary terms and $LS_x = iLS_y$, the z axis being the internuclear axis.

The electronic energies, the transition dipole moment between $X^1\Sigma_g^+$ and $A^1\Sigma_u^+$, and the spin-orbit coupling elements LS_y and $-iLS_z$ were fitted by 14th order polynomial expansions of morse-type coordinate,

$$Q = 1 - \exp[-0.3(r - r_e)]$$

the 0.3 exponent being found suitable for all the functions. r_e is the equilibrium internuclear distance of the given electronic state. For the coupling functions, r_e is chosen to be the equilibrium internuclear distance of the electronic ground state $X^1\Sigma^+$.

The coefficients of the potential fits are given in Table 2. Note that the first coefficient gives the

relative energetic position of the functions and we included in Table 2 a "shifted" coefficient that was used in all the bound states and dynamical calculations in order to fit the correct experimental transition energies (see below in Table 3). Figure 1 shows the energy of the three electronic states as a function of internuclear distance. The crossing of the $A^1\Sigma_u^+$ and $b^3\Pi_u$ states occurs at $r = 7.02$ bohr.

==========

Table 2 and Figure 1 near here

==========

Equilibrium geometries, r_e, of the three electronic functions are given in Table 3, with other spectroscopic data. In order to compare our results to previous RKR potentials, we also derived the harmonic wavenumbers, ω_e, and the anharmonic constants, $\omega_e x_e$ [24], the equilibrium rotational constants, B_e, the dissociation energies D_e and **the energy differences between the ground state and each excited state equilibrium positions, T_e.**
For comparison, non-relativistic CCSD(T) [25, 26] calculations on the electronic ground state correlating the sub-shells $2s$, $2p$ and $3s$ of each Na atoms have been carried out using the cc-pCVQZ [27] basis set. The corresponding values of $r_e = 5.835$ bohr and $\omega_e = 158.3$ cm$^{-}1$ are in nice agreement with the ECP + CPP / MRCI results which validates the accuracy of the present *ab initio* **ECP + CPP / MRCI potentials. For these potentials, Table 3 shows** that the equilibrium distances are always smaller by 0.01-0.02 bohr than the experimental values, the harmonic wavenumbers larger by 1-2 cm^{-1} and the energies D_e are always smaller by 80-200 cm^{-1}. The discrepancies are stronger for the spectroscopic constants of the $A^1\Sigma_u^+$ state due the flatness of the potential. The equilibrium transition energies, T_e, are 13 cm^{-1} below the experimental value for $b^3\Pi_u$ and 78 cm^{-1} for $A^1\Sigma_u^+$. The error in T_e value is different for each state because the correlation energy treatment is different for single and triplet electronic states in MRCI. However, our results are in better agreement with experimental data than previous accurate *ab initio* data obtained by Magnier *et al.* [8] using configuration interaction calculations and pseudopotentials. The energy difference between the $X^1\Sigma_g^+$ and $b^3\Pi_u$ electronic states at dissociation gives 16872 cm^{-1} which is in good agreement with the experimental value of 16956 cm^{-1} determined by Moore [22] for the energy difference between X ^2S and A ^2P electronic states of Na.

==========

Table 3 near here

==========

The coefficients for the fits of the coupling functions are given in Table 4. The transition dipole moment between $X^1\Sigma_g^+$ and $A^1\Sigma_u^+$ is plotted for r between 3 and 20 bohr in Figure 2 and is compared with other calculations [12, 13]. The three curves present a similar behavior for values of r up to r_e and our function is very close to recent *ab initio* data from Ahmed *et al.* [13] who calculated the transition dipole moment with the method used by Magnier *et al.* [8] for the electronic states. For larger values of r the theoretical data of Konowalow *et al.* [12] obtained at the MCSCF level does not tend towards the experimental atomic limit [12] of -3.56 ± 0.11 a.u. in contrary to the other *ab initio* functions. The transition dipole moment displays an almost linear behavior in the Franck Condon region of the ground state, around 6 bohr, but this approximation will not remain valid if one chooses to study transitions from an excited vibrational state of the ground electronic state that reaches broader part of the configuration space.

==========

Figure 2 and Table 4 near here

==========

The spin-orbit coupling elements between $A^1\Sigma_u^+$ and $b^3\Pi_u$ are shown in Figure 3. Their variation in the crossing region of these two electronic states is very small and a linear approximation might again give reasonable results although we used the computed couplings in the calculations of the next sections. Up to now, no geometry dependent coupling was published. However, Dulieu and Julienne [15] used a variable function for the fine structure coupling $2LS_y$ which varies from $\sqrt{2}/3\Delta E_{FS} = 8.11$ cm^{-1} for $r \to \infty$ to 5.47 cm^{-1} for $r = 8.5$ bohr, where $\Delta E_{FS} = 17.1963$ cm^{-1} is the atomic fine structure splitting of the first ^{2}P state of Na [22]. Our *ab initio* calculations give $\Delta E_{FS} = 17.21$ cm^{-1} and $2LS_y = 8.1$ cm^{-1} at $r \to \infty$, $2LS_y = 5.48$ cm^{-1} at $r = 8.5$ bohr and $2LS_y = 6.01$ cm^{-1} at $r = 7.02$ bohr (the crossing point of the potential electronic curves of $A^1\Sigma_u^+$ and $b^3\Pi_u$). These values are in remarkable agreement due to the fact that the parameters of the pseudopotential (see Table 1) were fitted in orderto reproduce as closely as possible the atomic spin-orbit splitting. These values can also be compared to experimental values extracted from vibrational analysis giving constant couplings of 5.91±0.14 cm^{-1} , 5.769±0.006 cm^{-1} and 5.97±0.15 cm^{-1} [5, 14, 28].

==========

Figure 3 near here

==========

In the basis of $^1\Sigma_u^+, M_S = 0$; $^3\Pi_{ux}, M_S = 1, 0, -1$; $^3\Pi_{uy}, M_S = 1, 0, -1$, the sum of the scalar-relativistic electronic Hamiltonian, $\hat{H}_{el}$ and the spin-orbit coupling operator, $\hat{H}_{SO}$ is associated to the matrix :

$$\mathbf{H_{el}} + \mathbf{H_{SO}} = \begin{pmatrix} V(^1\Sigma_u^+) & LS_y & 0 & LS_y & LS_x & 0 & -LS_x \\ LS_y & V(^3\Pi_u) & 0 & 0 & LS_z & 0 & 0 \\ 0 & 0 & V(^3\Pi_u) & 0 & 0 & 0 & 0 \\ LS_y & 0 & 0 & V(^3\Pi_u) & 0 & 0 & -LS_z \\ -LS_x & -LS_z & 0 & 0 & V(^3\Pi_u) & 0 & 0 \\ 0 & 0 & 0 & 0 & 0 & V(^3\Pi_u) & 0 \\ LS_x & 0 & 0 & LS_z & 0 & 0 & V(^3\Pi_u) \end{pmatrix}$$

The eigenfunctions of $\hat{L}_z$, labeled $|M_L, M_S\rangle$,

$$|0,0\rangle = |^1\Sigma_u^+, M_S = 0\rangle$$

$$|\pm 1, j\rangle = \frac{1}{\sqrt{2}}\left[|^3\Pi_{ux}, M_S = j\rangle \pm i|^3\Pi_{uy}, M_S = j\rangle\right]$$

with $j = 1, 0$ or -1, are introduced. In the basis $\{|0,0\rangle, |1,-1\rangle, |-1,1\rangle, |-1,0\rangle, |1,0\rangle, |-1,-1\rangle, |1,1\rangle\}$, and using the fact that $LS_x = iLS_y$, the above matrix becomes:

$$\mathbf{H'_{el}}+\mathbf{H'_{SO}} = \begin{pmatrix} V(^1\Sigma_u^+) & \sqrt{2}LS_y & \sqrt{2}LS_y & 0 & 0 & 0 & 0 \\ \sqrt{2}LS_y & V(^3\Pi_u) - iLS_z & 0 & 0 & 0 & 0 & 0 \\ \sqrt{2}LS_y & 0 & V(^3\Pi_u) - iLS_z & 0 & 0 & 0 & 0 \\ 0 & 0 & 0 & V(^3\Pi_u) & 0 & 0 & 0 \\ 0 & 0 & 0 & 0 & V(^3\Pi_u) & 0 & 0 \\ 0 & 0 & 0 & 0 & 0 & V(^3\Pi_u) + iLS_z & 0 \\ 0 & 0 & 0 & 0 & 0 & 0 & V(^3\Pi_u) + iLS_z \end{pmatrix}$$

This matrix is now block-diagonal and highlights the fact that the $b^3\Pi_u$ state splits into 6 components labeled Ω = 2, 1, 0, 0, -1, -2 due to internal spin-orbit coupling. The $|\Omega| = 2$ components are associated with $|-1,-1\rangle, |1,1\rangle$ and the $|\Omega| = 1$ with $|-1,0\rangle, |1,0\rangle$ respectively. The spin electronic components of the $b^3\Pi_u$ which interacts with $A^1\Sigma_u^+$ via spin-orbit coupling are: $|1,-1\rangle$ and $|-1,1\rangle$ corresponding to $\Omega = 0$. If the linear combinations of these components are used to express $\hat{H}_{el}+\hat{H}_{SO}$, the following matrix is obtained in the basis $\{|0,0\rangle, \frac{1}{\sqrt{2}}\left[|1,-1\rangle + |-1,1\rangle\right], \frac{1}{\sqrt{2}}\left[|1,-1\rangle - |-1,1\rangle\right]\}$:

$$\mathbf{H''_{el}} + \mathbf{H''_{SO}} = \begin{pmatrix} V(^1\Sigma_u^+) & 2LS_y & 0 \\ 2LS_y & V(^3\Pi_u) - iLS_z & 0 \\ 0 & 0 & V(^3\Pi_u) - iLS_z \end{pmatrix}$$

This matrix confirms that the only spin electronic component of $b^3\Pi_u$ which interacts with $A^1\Sigma_u^+$ via spin-orbit coupling is $\Omega = 0^+$ corresponding to

$$|^3\Pi_u(\Omega = 0^+)\rangle = \frac{1}{2}\left[-|^3\Pi_{ux}, M_S = 1\rangle - |^3\Pi_{ux}, M_S = -1\rangle + i|^3\Pi_{uy}, M_S = 1\rangle - i|^3\Pi_{uy}, M_S = -1\rangle\right]$$

This interaction creates an avoided crossing between the two states. In order to reduce the number of spin-electronic states involved in the dynamics presented in the next sections, the preceeding matrix is reduced into a two dimensional space containing only the $\Omega = 0^+$ component of $b^3\Pi_u$ and the $A^1\Sigma_u^+$ state. The reduced matrix in the basis of $^1\Sigma_u^+(\Omega = 0^+)$, $^3\Pi_u(\Omega = 0^+)$ is:

$$\mathbf{H_{el}} + \mathbf{H_{SO}} = \begin{pmatrix} V(^1\Sigma_u^+) & 2LS_y \\ 2LS_y & V(^3\Pi_u) - iLS_z \end{pmatrix}$$

This diabatic representation of two coupled states was used in the following wave packet study.

3 Vibrational states determination

We computed bound vibrational states on the ground $^1\Sigma_g^+$, the $A^1\Sigma_u^+$, the $b^3\Pi_u$ and the $b^3\Pi_u(\Omega = 0^+)$ states using a Lanczos diagonalisation scheme [29] on a grid of 512 points between 2.5 and 20 bohr. Experimental energies of the $A^1\Sigma_u^+$ bound states were compiled by Gerber and Möller [10] and used to create a RKR potential for this electronic state, and a RKR potential for the $b^3\Pi_u$ state was established by Whang *et al.* [11]. Table 5 shows the energies determined from our potentials and the RKR energies. The RKR potentials were made from experimental data associated to highly excited rovibrational states, and spin-orbit deperturbated in order to get uncoupled $A^1\Sigma_u^+$ and $b^3\Pi_u$ states. There is a nice agreement between experimental and theoretical values although the difference tends to slowly increase up to 22 cm^{-1} at $v = 20$ for the singlet and up to 11 cm^{-1} at $v = 20$ for the triplet showing that our potentials are slightly less anharmonic than the RKR potentials. The energy splitting, A_v, in the normal spin-orbit multiplet of a $b^3\Pi_u$ vibrational state before interaction with the $A^1\Sigma_u^+$ state has been derived by Shimizu and Shimizu [6] in a perturbative expansion as a function of v :

$$A_v = A_e + \alpha_A(v + \frac{1}{2})$$

where $A_e = 7.08 \pm 0.06$ cm^{-1} and $\alpha_A = -0.0156 \pm 0.0034$ cm^{-1}.

In our case A_v can be evaluated from the difference between the numbers in the columns associated with $b^3\Pi_u$ and $b^3\Pi_u(\Omega = 0^+)$ of Table 5 since the $b^3\Pi_u$ is associated with the unperturbed terms $b^3\Pi_u(\Omega = \pm 1)$. A linear regression of this difference as a function of $(v + 1/2)$ gave values of $A_e = 7.13$ cm^{-1} and $\alpha_A = -0.0171$ cm^{-1} in agreement with Shimizu and Shimizu [6] numbers. This nice agreement shows that our LS_z function is of good quality in a large part of configuration space, spanned by highly excited vibrational states.

==========

Table 5 near here

==========

The spin-orbit coupling between $A^1\Sigma_u^+$ and $b^3\Pi_u$ has been experimentally studied with great accuracy by Effantin *et al.* [5] who obtained state to state spin-orbit interaction parameters, $\xi_{vv'}$, defined by

$$\xi_{vv'} = \langle {}^1\Sigma_u^+, v|2LS_y|{}^3\Pi_u(\Omega = 0^+), v'\rangle.$$

Using eigenstates obtained in the previous section and the spin-orbit coupling function of Table 4, we computed $\xi_{vv'}$ for v values from $v = 0$ to $v = 17$ and v' values from $v' = 0$ to $v' = 50$. The largest value is $\xi_{0,5} = 2.67$ cm^{-1} but it is interesting to note that $\xi_{vv'}$ remains non negligible for a broad set of v and v' numbers and that the general coupling scheme does not seem to be reduced to the coupling of a particular $A^1\Sigma_u^+$ vibrational state to a particular $b^3\Pi_u$ vibrational state. For example $\xi_{0,v'} > 10^{-2}$ cm^{-1} for v' values up to $v' = 16$ and $\xi_{17,v'} > 10^{-2}$ cm^{-1} for all $v' < 40$. Table 6 shows a selection of $\xi_{vv'}$ compared to those obtained by Effantin *et al.* The agreement is again very nice, showing the good quality of the LS_y component of the spin orbit term, and of the calculated wavefunctions.

==========

Table 6 near here

==========

4 Time dependent analysis

In order to further check the validity of our electronic calculations, we tried to simulate the time resolved experiment of Rutz *et al.* [4]. A pump laser pulse excites the molecule from the ground electronic state of Na_2 to the $A^1\Sigma_u^+$ state and a probe pulse identical to the pump ionizes the excited molecule to the ground state of Na_2^+ via a two photon process involving the $^1\Pi_g$ state. The ion signal is measured as a function of the delay between the pump and probe pulses and an oscillatory pattern is obtained, reflecting the oscillating movement of the wave packet on the $A^1\Sigma_u^+$ surface. An analysis of this signal gives information on the position of the vibrational energy levels of the system, and the influence of the spin-orbit coupling on the level positions is detected when the pulse carrier frequency is set to $\lambda = 642$ nm but is not seen for $\lambda = 620$ nm. These values of excitation energies are associated with resonances of the ionization step when the wave packet is at the outer or inner classical turning point of the $A^1\Sigma_u^+$ state, respectively.

We used the Short Iterative Lanczos (SIL) [30] algorithm to propagate the wave packet on the three coupled states. The grid is the same as the one used in bound states determination above and the initial wave packet is the ground vibrational state of the ground electronic state, a reasonable guess since the vibrational temperature in the experiment is between 10 K and 50 K. The pump pulse

is the same one as in the experiment and we carried out the evolution for times up to 3 ps. The experimental pump-probe pulse delays of ref [4] varies up to 60 ps, but the few oscillations that we describe with our propagation are sufficient to discuss most of the features observed. The probing part of the experiment was not simulated but the wave packet evolving on the $A^1\Sigma_u^+$ contains all the relevant information.

The theoretical oscillation period was computed from the oscillations of the expectation value of the bond length as a function of time. This value is equal to the measured oscillation period, especially during the first oscillations, when the wave packet spreading has not taken place. We used a pulse identical to the experimental one with a sech^2 envelope (FWHM= 110 fs, peak power 0.5 GW cm^{-2}) and a given wavelength, λ. The complete pulse has the form

$$E(t) = A\ \text{sech}^2[\alpha(t - t_0)]\cos(2\pi t/\lambda)$$

Table 7 summarizes the pulse parameters used in our calculations and the theoretical and experimental oscillation periods. A good agreement is obtained, indicating that the first step of the process, i.e. the transition from the ground electronic state to the $A^1\Sigma_u^+$ state is well described in our simulation.

==========

Table 7 near here

==========

The next step is the analysis of the populations of the vibrational levels of the $A^1\Sigma_u^+$ and $b^3\Pi_u(\Omega = 0^+)$ states, done by projecting the time dependent wave packet $|\psi(t)\rangle$ on the previously computed eigenstates $|\psi_v\rangle$

$$|c_v(t)|^2 = |\langle\psi(t)|\psi_v\rangle|^2$$

In the $\lambda = 620$ nm experiment, the most populated states are in the $v = 12$ to $v = 14$ range in the $A^1\Sigma_u^+$ electronic state and no effect of the spin-orbit coupling was detected. This is in agreement with our calculations (see figure 4). These levels are populated during the pulse duration (roughly 250 fs) and the population of all the triplet vibrational states are below $5 \cdot 10^{-4}$, even after 3 ps when the wave packet has reached the coupling region several times in its oscillating movement.

In the $\lambda = 642$ nm experiment, the most populated states are in the $v = 7$ to $v = 9$ range and small deviations in the position of the lines were attributed to the spin-orbit coupling with triplet vibrational states around $v' = 14$. The plot of vibrational states population of the singlet (figure 5) shows an important increase of the population of $v = 7$ to $v = 9$ states during the pulse excitation

and the populations of the triplet state show an important increase in the population of $v' = 14$ state.

The first order perturbation term of two states coupled via spin-orbit interaction is

$$P_{vv'} = \frac{\xi^2_{vv'}}{E_v - E_{v'}}.$$

From Table 5, we can see that the energy difference between $v = 13$ and $v' = 18$ is less than 3 cm^{-1} and that the energy difference between $v = 8$ and $v' = 14$ is less than 6 cm^{-1}, indicating in both case a possibility of resonance. However, the $\xi_{vv'}$ coupling element from Table 6 is an order of magnitude stronger in the case of the $v = 8$ $v' = 14$ interaction which explains the larger population of this state in the $\lambda = 642$ nm experiment.

==========

Figure 4 and figure 5 near here

==========

The largest experimental energy shift [4] of a vibrational level on the $A^1\Sigma_u^+$ due to spin-orbit coupling was observed for $v = 8$. The value of the shift was evaluated at $\delta_8 = 0.8$ cm^{-1}. To obtain this shift, we must add the contribution of all the v' states to the perturbation of a given v state.

$$\delta_v = \sum_{v'} P_{vv'}$$

As noted above, states which are not in close energetic resonance may still contribute to the global shift of the level because the $\xi_{vv'}$ coupling terms remain non negligible for a large set of v and v' values. We obtain a global shift of $\delta_8 = 0.3$ cm^{-1}. A probable reason of the difference between this value and the experimental one is molecular rotation that was not taken into account in our dynamical approach. Experimental data shows that rovibrational states up to J=25 are involved in the process and the summation in the preceeding equation should be on rovibrational states rather than only vibrational states.

5 Conclusion

The *ab initio* potential, transition dipole moment and spin-orbit coupling for the electronic states were computed with high accuracy and form a coherent package of data that can be used to simulate dynamical processes involving these states. We were able to reproduce experimental results from Rutz *et al* [4] concerning the oscillating period of the wave packet on the $A^1\Sigma_u^+$ state for two different excitation frequencies from the ground electronic state and the pattern of coupling between

vibrational levels of the $A^1\Sigma_u^+$ and $b^3\Pi_u(\Omega = 0^+)$ states for these excitations. We also found that one wavelength lead to observation of spin-orbit coupling effects while the other did not, but the exact determination of energy level displacements would need to include rotational motion in the dynamical calculations.

References

[1] E.-B. W. Lerch, X. Dai, S. Gilb, E. A. Torres and S. R. Leone, *J. Chem. Phys.*, **124**, 044306 (2006).

[2] L. Belau, J. Gorodetsky and Y. Haas, *J. Chem. Phys.*, **122**, 224318 (2005).

[3] S. Beyvers, Y. Ohtsuki and P. Saalfrank, *J. Chem. Phys.*, **124**, 234706 (2006).

[4] S. Rutz, S. Greschik, E. Schreiber and L. Wöste, *Chem. Phys. Lett.*, **257**, 365-373 (1996).

[5] C. Effantin, O. Babaky, K. Hussein, J. d'Incan and R.F. Barrow, *J. Phys. B*, **18**, 4077-4087 (1985).

[6] K. Shimizu and F. Shimizu, *J. Chem. Phys.*, **78**, 1126 (1983).

[7] D. D. Konowalow, M. E. Rosenkrantz and M. L. Olson, *J. Chem. Phys.*, **72**, 2612 (1980).

[8] S. Magnier, Ph. Millié, O Dulien and F. Manov-Seeuws, *J. Chem. Phys.*, **98**, 9 (1993).

[9] R. F. Barrow, J. Verges, C. Effantin, K. Hussein and J. d'Incan, *Chem. Phys. Letters*, **104**, 179 (1984).

[10] G. Gerber and R. Möller, *Chem. Phys. Letters*, **113**, 546 (1985).

[11] T.-J. Whang, W.C. Stawlley, L. Li and A.M. Lyyra, *J. Chem. Phys.*, **97**, 7211 (1992).

[12] D. D. Konowalow, M. E. Rosenkrantz and D. S. Hochhauser, *J. Mol. Spectro.*, **99**, 321-338 (1983) and references therein.

[13] E. Ahmed, A. Hansson, P. Qi, T. Kirova, A. Lazoudis, S. Kotochigova, A.M. Lyyra, L. Li, J. Qi and S. Magnier, *J. Chem. Phys.*, **124**, 84308 (2006).

[14] A.A. Stolyarov, I.P. Klincare, M.Y. Tamanis and R.S. Ferber, *J. Chem. Phys.*, **98**, 826 (1993).

[15] O. Dulieu and P.S. Julienne, *J. Chem. Phys.*, **103**, 60 (1995).

[16] MOLPRO, a package of ab initio programs designed by H.-J. Werner and P.J. Knowles *et al.*, version 2002.1, www.molpro.net.

[17] P. Fuentealba, L. v. Szentpaly, H. Preuss and H. Stoll, *J. Phys. B*, **18**, 1287 (1985).

[18] H.-J. Werner and P.J. Knowles, *J. Chem. Phys.*, **89**, 5803 (1988).

[19] P.J. Knowles and H.-J. Werner, *Chem. Phys. Lett.*, **145**, 514 (1988).

[20] H.-J. Werner and P.J. Knowles, *J. Chem. Phys.*, **82**, 5053 (1985).

[21] P.J. Knowles and H.-J. Werner, *Chem. Phys. Lett.*, **115**, 259 (1985).

[22] Ch. E. Moore, *Atomic Energy Levels, Vol. I*, Circular of the National Bureau of Standards 467, U.S. Government Printing Office, Washington, DC, 1949.

[23] K. G. Dyall, I. P. Grant, C. T. Johnson, F. A. Parpia and E. P. Plummer, *Comput. Phys. Commun.*, **55**, 425-456 (1989). GRASP: atomic numerical MCDHF package.

[24] D. Papousek and M.R. Aliev, *Molecular vibrational-rotational spectra*, Elsevier Scientific Publishing Company, 1982, page 160.

[25] C. Hampel, K. Peterson, and H.-J. Werner, *Chem. Phys. Lett.*, **190**, 1 (1992) and references therein.

[26] M. J. O. Deegan and P. J. Knowles, *Chem. Phys. Lett.*, **227**, 321 (1994).

[27] D. E. Woon, K. A. Peterson and T. H. Dunning, Jr. (to be published).

[28] H. Kato, M. Otani and M. Baba, *Chem. Phys.*, **89**, 653 (1988).

[29] J. K. Cullum and R. A. Willoughby, *Lanczos algorithm for large symmetric eigenvalue computation*, Birkhäuser, Boston, 1989.

[30] T. J. Park, J. C. Light, *J. Chem. Phys.*, **85**, 5870 (1986).

Figure captions:

Figure 1: Variation of the potential energy of the $X^1\Sigma_g^+$, $A^1\Sigma_u^+$ and $b^3\Pi_u(\Omega = 0^+)$ electronic states of Na_2 with the internuclear distance.

Figure 2: Variation of the transition dipole moment between the $X^1\Sigma_g^+$ and $A^1\Sigma_u^+$ electronic states of Na_2 with the internuclear distance r, compared to previous ab-initio data from by Ahmed *et al.* [13] and Konowalow *et al.* [12].

Figure 3: Variation of the spin-orbit coupling elements between the $A^1\Sigma_u^+$ and $b^3\Pi_u$ electronic states of Na_2 with the internuclear distance.

Figure 4: Population of the most populated vibrational levels on a) $A^1\Sigma_u^+$ and b) $b^3\Pi_u$ after excitation at $\lambda = 620$ nm.

Figure 5: Population of the most populated vibrational levels on a) $A^1\Sigma_u^+$ and b) $b^3\Pi_u$ after excitation at $\lambda = 642$ nm.

Table 1: Coefficients B and exponents β of the one-component ($\hat{V}^{SDF}$, [17]) and spin-orbit ($\hat{V}^{SO}$) pseudopotential for Na.

l	B	β
$\hat{V}^{SDF}$		
0	10.839000	1.378000
1	2.303000	0.663900
2	-1.777000	0.924900
$\hat{V}^{SO}$		
1	0.015867	0.663900
2	-0.001224	0.924900

Table 2: Polynomial expansion coefficients of the electronic energies (in hartree) of the $X^1\Sigma_g^+$, $A^1\Sigma_u^+$, $b^3\Pi_u$ electronic states of Na_2. The C_0' value shifts the surfaces in agreement with experimental transition energies of Table 3. The reference geometry, r_e for each fit comes from Table 3.

Coefficients	$X^1\Sigma_g^+$	$A^1\Sigma_u^+$	$b^3\Pi_u$
C_0	0.0000000	0.0665337	0.0615407
C_0' (shifted)	0.0000000	0.0668900	0.0616059
C_1	0.0000000	0.0000000	0.0000000
C_2	0.0617822	0.0343059	0.0580193
C_3	-0.0080603	0.0059603	0.0022293
C_4	-0.0148589	-0.0002812	-0.0021897
C_5	0.0035000	-0.0139701	0.0010511
C_6	-0.0028511	-0.0007393	-0.0123866
C_7	-0.0320161	0.0317575	-0.0048414
C_8	-0.0260680	0.0190173	0.0288718
C_9	0.0263861	-0.0201986	0.0114992
C_{10}	0.0377679	-0.0235446	-0.0455860
C_{11}	-0.0012869	-0.0032285	-0.0375163
C_{12}	-0.0148540	0.0049402	0.0135731
C_{13}	-0.0031591	0.0024082	0.0232065
C_{14}	0.0008343	0.0003337	0.0065160
RMS error($\times 10^{-6}$)	1.31	18.27	1.60

Table 3: Equilibrium geometries (/bohr) and spectroscopic constants (/cm^{-1}) of the $X^1\Sigma_g^+$, $A^1\Sigma_u^+$, $b^3\Pi_u$ electronic states of Na_2.

State		r_e	ω_e	$\omega_e x_e$	B_e	D_e	T_e
$X^1\Sigma_g^+$	RKR[a]	**5.818631***	**159.17732**	**0.760159**	**0.1546855**	6022.6	
	Theo. A [b]	5.83	156.8			5892	
	Theo. B [b]	5.77	159.3			5725	
	ECP+CPP/MRCI	**5.7995**	**159.893**	0.7487	0.1557	5950	
$A^1\Sigma_u^+$	RKR[c]	6.87474	117.2703	0.3534801	0.1108142	8310	14680.682
	Theo. A [b]	6.86	117.5			8284	14575
	Theo. B [b]	6.85	119.5			8118	14581
	ECP+CPP/MRCI	**6.8593**	**119.147**	0.3810	0.1113	8068	14602
$b^3\Pi_u$	RKR[d]	5.87075	154.209	0.47682	0.15195	9475.3	13520.946
	Theo. A [b]	5.87	154.6			9411	13447
	Theo. B [b]	5.81	153.0			9396	13304
	ECP+CPP/MRCI	**5.8561**	**154.946**	0.4722	0.1527	9316	13507

[a] Ref. [9], [b] Ref. [8] [c] Ref. [10], [d] Ref. [11].

* calculated from B_e.

Table 4: Polynomial expansion coefficients of the transition dipole moment between the $X^1\Sigma_g^+$, $A^1\Sigma_u^+$ electronic states and of the spin-orbit coupling between the $A^1\Sigma_u^+$ and $b^3\Pi_u$ electronic states of Na_2.

Coefficients	Dipole moment (a.u.)	LS_y ($/10^{-5}$) (a.u.)	-iLS_z ($/10^{-5}$) (a.u.)
C_0	-3.662650	1.635586	-2.286497
C_1	-1.005127	-1.012301	2.009225
C_2	-0.685894	0.350559	-0.908788
C_3	-0.172353	0.748145	-0.006000
C_4	1.694909	-0.649386	-0.344029
C_5	4.232320	-4.163085	-2.639413
C_6	-3.950725	3.259819	1.915624
C_7	-12.639680	16.838510	9.289735
C_8	11.693785	-4.351840	-3.316573
C_9	29.699469	-31.730642	-18.524042
C_{10}	-8.743500	-1.191377	-0.961422
C_{11}	-33.603118	29.706639	16.776839
C_{12}	-4.957655	7.978938	5.141925
C_{13}	13.275650	-10.805054	-5.429050
C_{14}	5.234212	-4.774218	-2.496550
RMS error	0.00084	9.92×10^{-9}	4.11×10^{-9}

Table 5: Vibrational states energies ($/cm^{-1}$) of the $X^1\Sigma_g^+$, shifted $A^1\Sigma_u^+$, shifted $b^3\Pi_u$ and $b^3\Pi_u(\Omega = 0^+)$ (obtained from shifted $b^3\Pi_u$) electronic states of Na_2.

Level v	$X^1\Sigma_g^+$	$A^1\Sigma_u^+$	$A^1\Sigma_u^+$[10]	$b^3\Pi_u$	$b^3\Pi_u$ [11]	$b^3\Pi_u(\Omega = 0^+)$
0	79.52	14741.89	14739.24	13597.70	13597.92	13590.57
1	237.96	14859.60	14855.80	13751.84	13751.18	13744.73
2	394.91	14976.61	14971.66	13904.98	13903.48	13897.89
3	550.36	15092.92	15086.81	14057.14	14054.82	14050.06
4	704.31	15208.52	15201.25	14208.30	14205.21	14201.24
5	856.74	15323.41	15314.99	14358.47	14354.64	14351.43
6	1007.55	15437.58	15428.02	14507.65	14503.12	14500.63
7	1156.98	15551.03	15540.34	14655.83	14650.64	14648.83
8	1304.76	15663.75	15651.97	14803.03	14797.20	14796.04
9	1450.96	15775.73	15762.88	14949.23	14942.80	14942.26
10	1595.57	15886.97	15873.10	15094.43	15087.44	15087.48
11	1738.53	15997.47	15982.61	15238.63	15231.12	15231.71
12	1879.93	16107.23	16091.42	15381.85	15373.83	15374.93
13	2019.64	16216.23	16199.53	15524.05	15515.58	15517.15
14	2157.68	16324.49	16306.94	15665.26	15656.36	15658.37
15	2294.03	16432.01	16413.65	15805.46	15796.17	15798.59
16	2428.66	16538.77	16519.66	15944.65	15935.00	15937.80
17	2561.54	16644.78	16624.97	16082.83	16072.86	16075.99
18	2692.66	16750.04	16729.58	16219.99	16209.74	16213.17
19	2821.97	16854.56	16833.49	16356.13	16345.64	16349.32
20	2949.46	16958.33	16936.70	16491.26	16480.55	16484.48

Table 6: State to state spin-orbit interaction parameters, $\xi_{vv'}(/\mathrm{cm}^{-1})$.

v	v'	$\xi_{vv'}$	$\xi_{vv'}$[5]
v=0	v'=6	2.60	2.50
v=0	v'=7	2.28	2.26
v=1	v'=7	1.39	1.39
v=1	v'=8	2.06	2.05
v=2	v'=8	0.53	0.51
v=2	v'=9	0.69	0.65
v=3	v'=9	1.61	1.58
v=4	v'=9	0.36	weak
v=4	v'=10	1.44	1.43
v=5	v'=11	0.44	0.42
v=6	v'=12	0.65	0.69
v=7	v'=12	1.12	1.15
v=7	v'=13	1.30	1.33
v=8	v'=14	1.30	-
v=9	v'=14	0.63	0.58
v=10	v'=15	1.17	1.17
v=13	v'=18	0.10	-

Table 7: Pulse parameters and oscillation period of the wave packet.

λ (/nm)	A (/a.u.)	α (/(fs^{-1}))	t_0 (/fs)	T_{calc}(/fs)	T_{exp}(/fs)
642	$1.194\ 10^{-4}$	$1.603\ 10^{-2}$	150	297	297
620	$1.194\ 10^{-4}$	$1.603\ 10^{-2}$	150	311	312

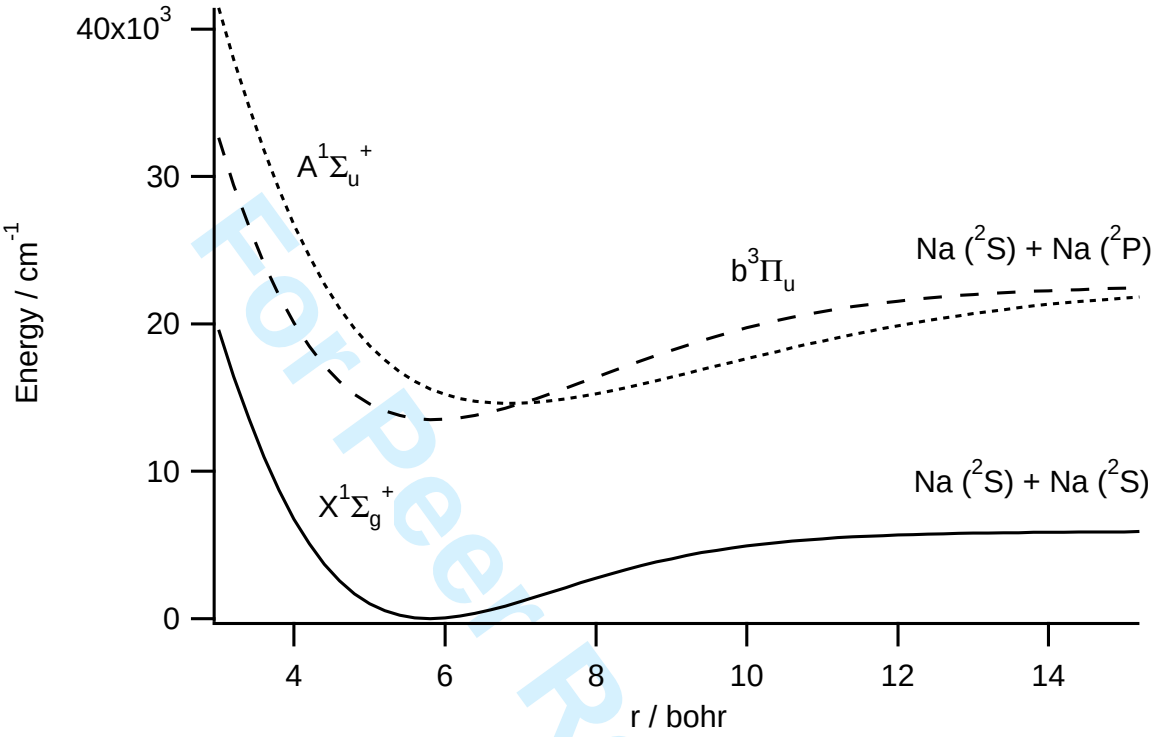

Figure 1

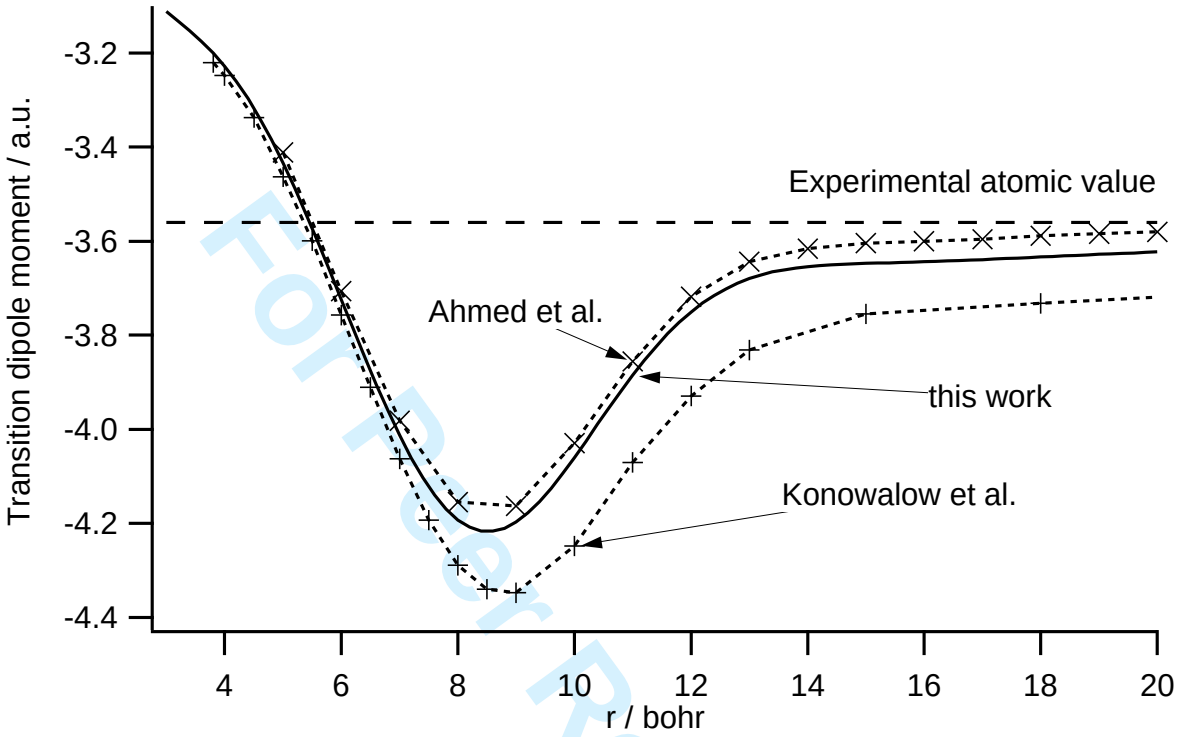

Figure 2

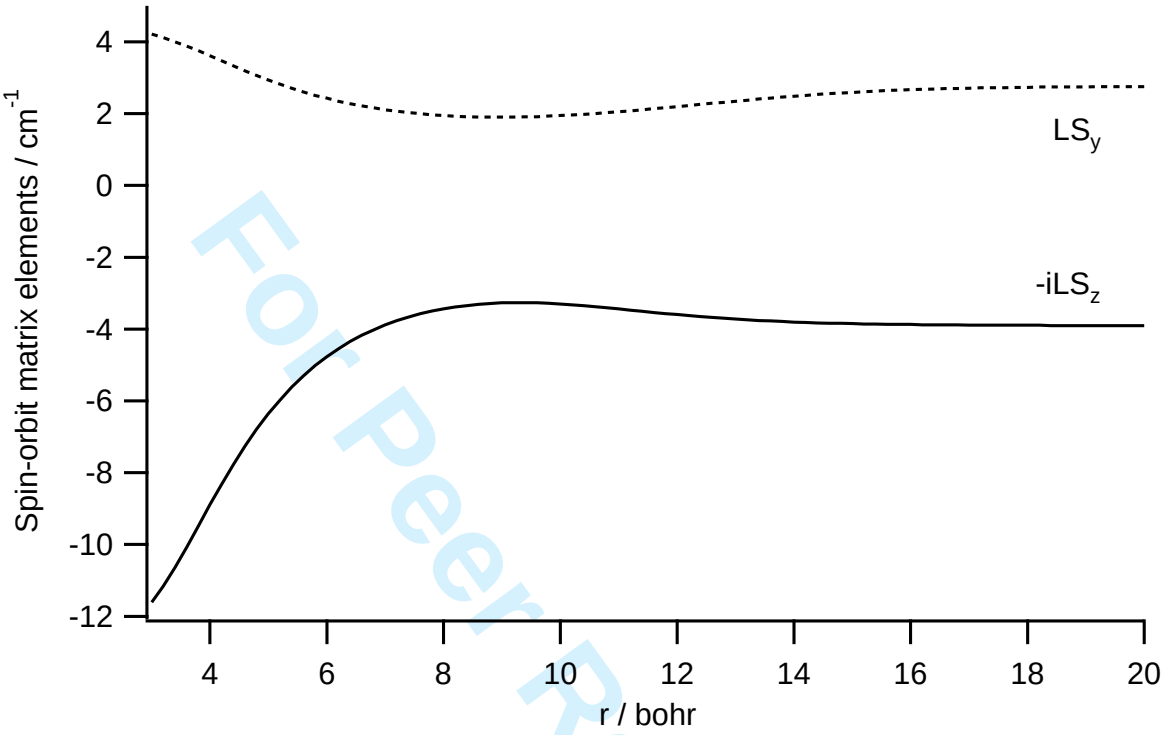

Figure 3

Figure 4

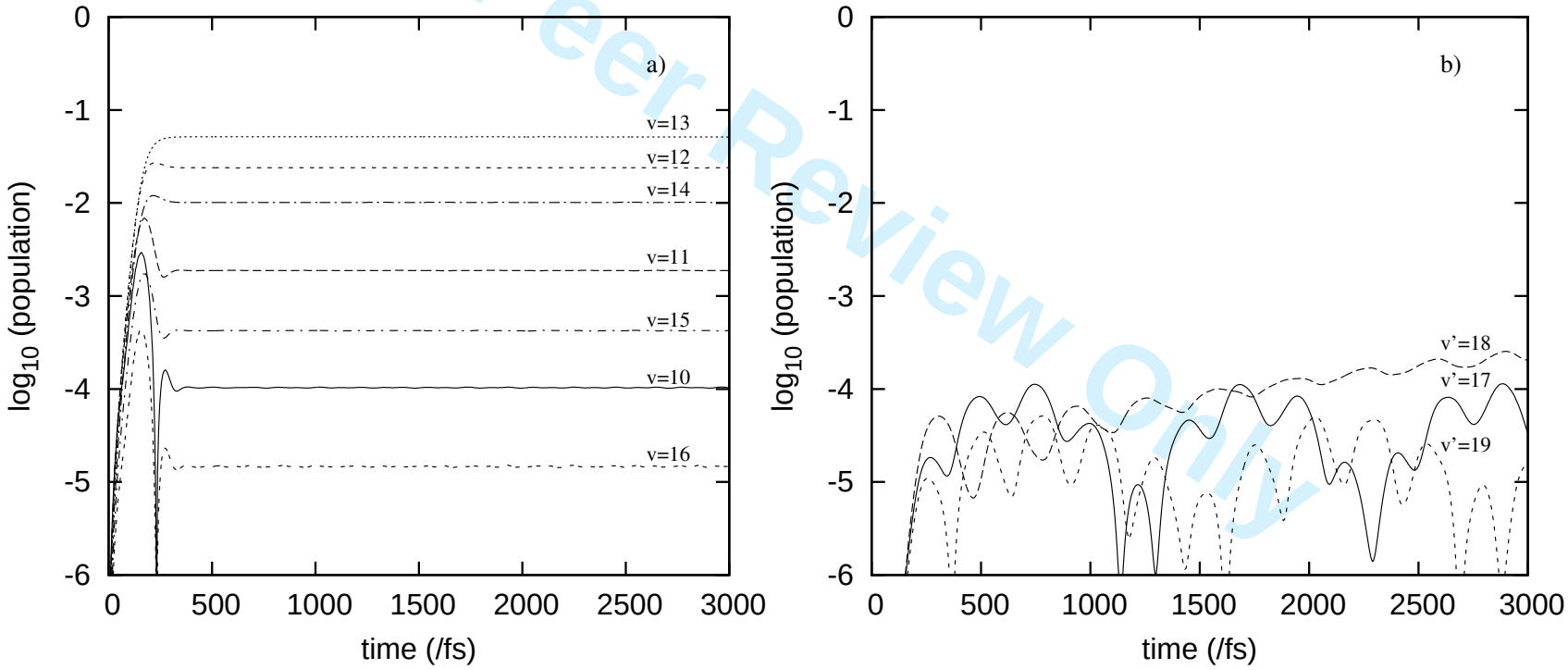

Figure 5